CAMBRIDGE
UNIVERSITY PRESS

# Article

# Differential dissolution of interlayer, octahedral and tetrahedral cations of vermiculite in oxalic acid

Yu Zhang, Hongjuan Sun*, Tongjiang Peng, Liming Luo and Li Zeng

Education Ministry Key Laboratory of Solid Waste Treatment and Resource Recycle, Southwest University of Science and Technology, Mianyang, China

## Abstract

Physical and/or chemical changes such as refinement, component dissolution, exchange/adsorption, structural evolution and recombination of phyllosilicate minerals occur continuously in a naturally weakly acidic water environment. To compare the differential dissolution of cations that occupy various sites in vermiculite, trioctahedral vermiculite was dissolved in various concentrations of oxalate for 24 h and in 0.2 M oxalate for various durations. The concentration of ions in the leaching solution and the phase, structure and morphology of the original samples and acid-leached samples were analysed. Structural analysis showed that the 001 reflections of vermiculite gradually shifted to a higher angle and eventually disappeared after the dissolution of interlayer cations caused by acid leaching. The amount and rate of dissolution of each cation in the vermiculite showed that the octahedral cation $Mg^{2+}$ is more soluble than $Fe^{2+}$ and $Fe^{3+}$. The dissolution rates of $Al^{3+}$, $Mg^{2+}$ and $Ca^{2+}$ were greatest in the first 4 h and then decreased gradually. Amorphous silicon dioxide and calcium oxalate were formed during acid leaching, and calcium oxalate was formed in the first 4 h. After leaching with oxalate for various periods, the cation-exchange capacity (CEC) of the samples first increased and then decreased. Micromorphology analysis showed that the acid erosion process started from the edges. The results of this work contribute to our understanding of many natural geochemical processes, and they will be useful for several applications such as soil improvement, ecological restoration and environmental protection.

Mineral–water interface reactions occur widely in nature. Inorganic acidic substances discharged by human beings or organic acidic substances discharged by plants and microorganisms come into contact with minerals through wet sedimentation or surface runoff. When minerals come into contact with an out-of-balance aqueous fluid, reactions begin as the system tries to establish a new equilibrium (Putnis & Ruiz-Agudo, 2013). Physical and chemical processes such as structural changes and component dissolution of minerals constantly occur in such weakly acidic systems. It has been found that the dissolution of mineral components is affected by the rate and duration of the mineral–water interface reaction and the properties of the minerals and water (White & Brantley, 2003). The dissolution of silicate minerals does not occur uniformly on all exposed surfaces but preferentially on some sites with weak structures or excess surface energy (e.g. dislocations, vacancies, microfractures, grain boundaries, *etc.*). Screw dislocation was found to play a significant role in determining surface topography evolution during dissolution (He *et al.*, 2019), and the existence of cavitation bubbles in the fluid was found to accelerate the dissolution rate of mineral crystals (Su & Zhou, 2020). Minerals with varying structures and compositions show various reaction rates during water interface reactions.

Vermiculite is composed of Mg(Fe, Al, *etc.*)O metal octahedral sheets (O) sandwiched by two Si(Al)O$_4$ tetrahedral sheets (T) and one or two hydrate layers between the TOT layers (Bailey, 1980; Guggenheim *et al.*, 2006). Due to isomorphic substitution ($Al^{3+}$ in the tetrahedron instead of $Si^{4+}$, $Fe^{3+}$ in the octahedron instead of $Mg^{2+}$, *etc.*) in the lattice, the layers have permanent negative charges that are compensated mainly by interlayer cations (Mittal, 2013). During interfacial reactions, the interlayer cations of vermiculite are replaced by $H_3O^+$. Acid etching, in turn, dissolves the octahedral sheet through the interlayers and the edges (Steudel *et al.*, 2009). Additionally, acid etching causes both holes and amorphous silica residues to form on the surface of the vermiculite (Suquet *et al.*, 1991; Frini-Srasra & Srasra, 2010). Maqueda *et al.* (2009) found that these residues consisted of silica and iron oxide and that the high surface area of the residues was probably due to the presence of iron. After mineral–water interfacial reactions, vermiculite not only exhibits greater porosity and both Brønsted and Lewis acidity (del Rey-Perez-Caballero & Poncelet, 2000), but also can produce porous silica with high specific surface area (Temuujin *et al.*, 2003; Maqueda *et al.*, 2007). The changes in the properties of vermiculite after acid interface reactions, such as increasing specific surface area (Victoria *et al.*, 2017) and decreasing layer charge (Warren *et al.*, 1992), are all caused by structural changes.

Vermiculite is widely distributed in nature, and its unique structure (unsaturated layer charge, large specific surface area, water in the structure, *etc.*) makes it adsorbable and ion

*Corresponding author: Hongjuan Sun; Email: sunhongjuan@swust.edu.cn

**Table 1.** Chemical composition of the vermiculite sample (wt.%).

| Sample | $SiO_2$ | $Al_2O_3$ | $K_2O$ | $TFe_2O_3$ | $Na_2O$ | CaO | MgO | $TiO_2$ | BaO | F | $Cr_2O_3$ |
|---|---|---|---|---|---|---|---|---|---|---|---|
| Ver-0 | 43.68 | 13.40 | 5.01 | 8.56 | 1.27 | 3.21 | 22.14 | 1.79 | 0.25 | 0.13 | 0.12 |

exchangeable, and these advantages mean that it is widely used in the fields of agriculture and environmental protection. Although there have been many studies on the acid treatment of vermiculite, there have been few studies on the reaction processes and mechanisms of vermiculite at oxalic acid interfaces. The purpose of this study is to investigate the dissolution rate of interlayer, octahedral and tetrahedral cations of Xinjiang Yuli vermiculite when reacted with acidic (oxalic acid) water for various periods and at various concentrations. The structural and morphological changes of vermiculite before and after treatment were analysed. This study provides a theoretical basis for understanding these geochemical processes and expands the effective utilization of vermiculite in the field of environmental protection.

## Materials and methods

### Samples

The vermiculite sample was obtained from Xinjiang Yuli and marked as Ver-0. The chemical composition of the vermiculite sample is shown in Table 1. $TFe_2O_3$ is the total iron oxide including FeO and $Fe_2O_3$. Based on the X-ray fluorescence (XRF) results, the structural formula of the sample was expressed as $(Ca_{0.15}K_{0.28}Na_{0.16}Ba_{0.01})[(Mg_{2.29}Fe_{0.45}Ti_{0.09}Al_{0.06}Cu_{0.07}Cr_{0.01})$ $(Si_{2.98}Al_{1.02})O_{10}(OH)_2]\cdot nH_2O$ using the structural formula method (Christidis, 2008), where $K^+$ could belong to the phlogopite in the vermiculite sample. The crystal chemical formula calculation indicated that the interlayer cations were mainly $Ca^{2+}$ and $Na^+$ and the octahedral cations were mainly $Mg^{2+}$, with small amounts of $Fe^{3+}$, $Ti^{4+}$ and $Cr^{3+}$. Tetrahedral cations were mainly $Si^{4+}$ and $Al^{3+}$.

### Sample preparation

The vermiculite sample was ground using a pestle and mortar and sieved using a 100 mesh sieve. Two sets of experiments were conducted. In the first set of experiments, 1 g of the sample was added to 50 mL of a 0.2 M $H_2C_2O_4$ solution and kept for different durations (4, 12, 24, 48 and 72 h) at room temperature. In the second set of experiments, 1 g of the sample was added to 50 mL of various concentrations (0.05, 0.1, 0.15, 0.2, 0.25 M) of a $H_2C_2O_4$ solution and kept for 24 h at room temperature. The conical flask was shaken at regular intervals to ensure the reaction proceeded smoothly. After filtration, samples were repeatedly washed with distilled water to remove any residual acid and then oven-dried at 60°C and ground.

The oxalic acid hexahydrate was purchased from Chengdu Kelong Chemical Co. Ltd (China). The water for experiment was self-made ultrapure water with resistivity >18.2 MΩ cm$^{-1}$.

### Characterization

Mineral-phase and structural analyses were performed using an X-ray diffractometer (XRD; D/max-IIIA, Rigaku, Japan) at room temperature using Ni-filtered radiation from a Cu tube. Measurements were performed at a voltage of 40 kV and a current

of 40 mA from 3 to 80°2θ at a rate of 20° min$^{-1}$ and a slit width of 0.6 mm.

The chemical composition of the raw material was analysed using an XRF spectrometer (Axios, PANalytical, The Netherlands). The samples were prepared using the fusible method, and the test conditions were a ceramic X-ray tube (Rh target) with a maximum power of 2.4 kW. Cation concentrations in the solution were measured using a Thermo iCAP 6500 inductively coupled plasma–atomic emission spectrometer (ICP-AES) with continuous wavelength coverage in the range 166–847 nm. The optical resolution was <0.007 nm at 200 nm wavelength.

Thermogravimetric and differential scanning calorimetry (TG-DSC) analyses were performed using a TA SDT Q160 instrument (TA Instruments, DE, USA). The samples were heated in alumina crucibles from 30°C to 1200°C at a rate of 10°C min$^{-1}$ under a constant overflow of $N_2$ (50 mL min$^{-1}$).

The surface morphology of the samples was investigated using a scanning electron microscope (SEM; Carl Zeiss Sigma 300, Germany) equipped with an X-ray dispersive energy spectrometer (EDS). The samples were coated with gold film before SEM investigation, and measurements were performed at a voltage of 15 kV.

Fourier-transform infrared (FTIR) spectra of the samples were recorded using a Nicolet-5700 model infrared spectrometer in the range of ~400–4000 cm$^{-1}$ at 20 scans and resolution of 2 cm$^{-1}$ (Thermo Nicolet, MA, USA). Samples were prepared using the KBr tablet pressing method. The specific surface area of the samples was determined using a specific surface area analyser (iQ Quantachrome, Autosorb, FL, USA) according to the multipoint Brunauer–Emmett–Teller (BET) method.

CEC of the treated samples was determined based on an ammonium chloride–ethanol exchange method: 0.01 g was added to a 100 mL centrifuge tube and the soluble salt of it was washed with ethanol. Then, 40 mL of an ammonium chloride solution was added and stirred for 2 h to make the ammonium ions fully exchange with the interlayer cations. The suspension was centrifuged for 7 min at 7000 rpm, and the sediment was collected and washed twice with ethanol. Finally, 25 mL of a calcium chloride formaldehyde solution and phenolphthalein indicator were added and titrated with sodium hydroxide. The volume of sodium hydroxide standard solution consumed by each sample was recorded, and the CEC of the sample was calculated using Equation 1:

$$CEC = (C \times V/G) \times 100 \qquad (1)$$

where CEC is measured in meq 100 g$^{-1}$, $C$ (mol L$^{-1}$) is the sodium hydroxide standard solution concentration, $V$ (mL) is the volume of the sodium hydroxide standard solution consumed and $G$ (g) is the weight of the sample.

## Results and discussion

### Structural analysis

The main phase of the original sample (Fig. 1) was trioctahedral vermiculite (PDF#01-074-1732; $d_{001} = 14.48$ Å, $d_{002} = 7.33$ Å,
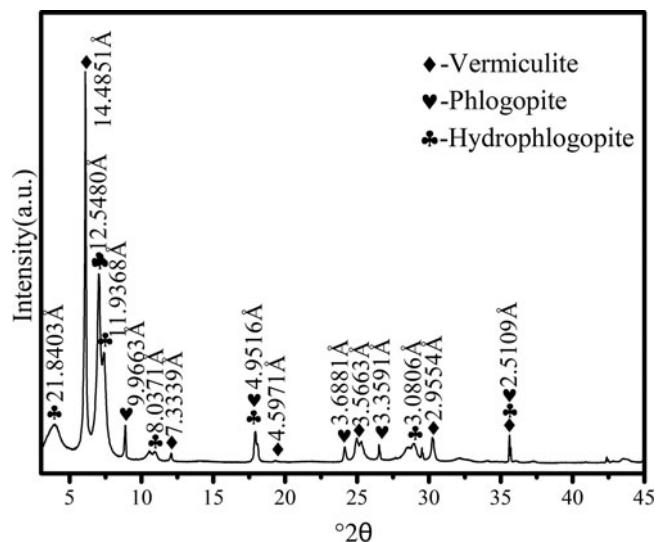
**Figure 1.** XRD traces of the vermiculite sample.

$d_{020} = 4.59$ Å, $d_{004} = 3.56$ Å; Ma *et al.*, 2019). Phlogopite (PDF#00-010-0495; $d_{001} = 9.96$ Å, $d_{002} = 4.95$ Å, $d_{003} = 3.35$ Å, $d_{004} = 2.51$ Å) and interstratified vermiculite–phlogopite (phl-ver; $d_{001} = 21.84$ Å, $d_{002} = 12.54$ Å, $d_{002} = 11.93$ Å, $d_{220} = 4.95$ Å) represent smaller percentages of the sample (Chambi-Peralta *et al.*, 2018).

XRD analysis was performed on the samples after the interfacial reaction of five concentrations of oxalate with vermiculite, and the results are shown in Fig. 2. Increasing the oxalic acid concentration changed the structure of the vermiculite samples significantly. Relative to the original sample, the 001 reflection of vermiculite gradually shifted to a higher angle because leaching
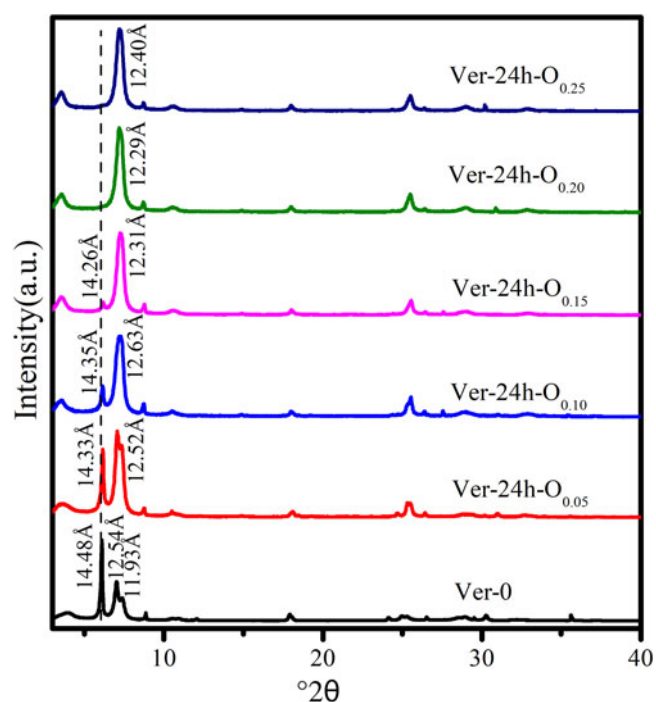
of the interlayer cations reduced the interlayer spacing. After leaching with oxalic acid of 0.05 and 0.15 M concentrations (Fig. 2), the interlayer spacing of vermiculite decreased from 14.48 Å to 14.33 Å and 14.26 Å, respectively. The reflection intensity of vermiculite at $d_{001} = 14.48$ Å decreased considerably compared to that of interstratified phl-ver at $d_{002} = 12.54$ Å. With increasing oxalic acid concentration, the reflection intensity of vermiculite at $d_{001} = 14.485$ Å gradually decreased, and the 001 reflection of vermiculite completely disappeared when the oxalic acid concentration was 0.2 M (Fig. 2). Under the same conditions, the diffraction peak (001) of interstratified phl-ver widened gradually. Therefore, increasing acid concentration led to the destruction of the structure of vermiculite and to a decrease in stacking regularity of interstratified phl-ver.

The XRD traces of the sample after 0.2 M oxalate interfacial reaction over various durations are shown in Fig. 3. After 12 h, due to the leaching of interlayer cations of vermiculite and the reduction of interlayer spacing, the layer spacing of $d_{001}$ was reduced from 14.51 to 14.41 Å. The diffraction peak (002) of interstratified phl-ver gradually widened because of the cation dissolution, and the layer spacing of $d_{001}$ of interstratified phl-ver was reduced from 12.58 to 12.01 Å after 72 h. After 24 h, the (001) reflection of vermiculite disappeared completely. The effect of acid leaching duration on the structure of the samples was that the degree of damage to vermiculite minerals was greater than to interstratified phl-ver.

## Cationic dissolution analysis

To facilitate the comparison with the measured chemical composition, the leaching rate of each metal cation was calculated by combining the volume of the acid solution and the mass of the sample. The results are shown in Fig. 4.
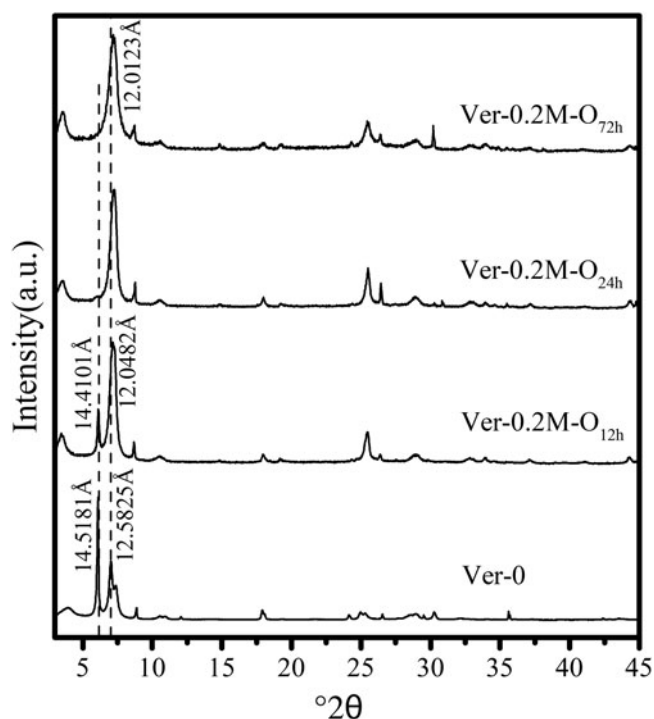


**Figure 2.** XRD traces of Ver-24h-On samples after leaching with various oxalate concentrations.



**Figure 3.** XRD traces of Ver-0.2M-Oₕ samples after leaching with 0.2 M oxalate at various durations.
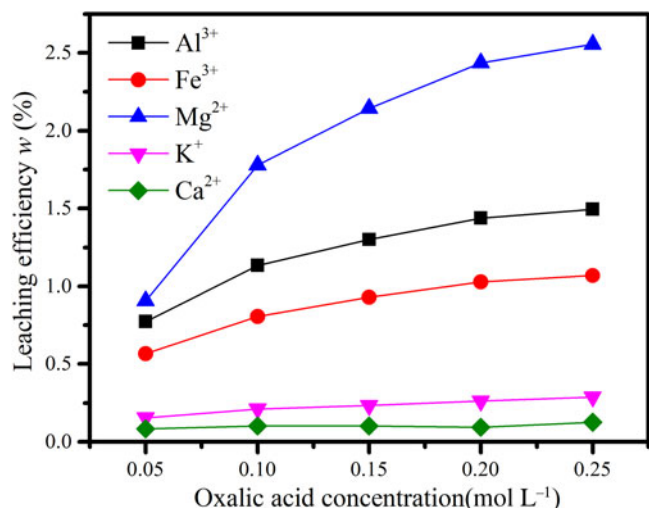
**Figure 4.** Dissolution amounts of cations of vermiculite at various concentrations of oxalic acid.

The metal cation dissolution amount was calculated using Equation 2:

$$w = \frac{a \times 10 \times 0.05}{1000} \div m \qquad (2)$$

where $w$ (%) is the dissolution amount of the cation, $a$ (mg L$^{-1}$) is the cation concentration, 10 is the dilution ratio, 0.05 (L) is the solution volume and $m$ (g) is the sample mass.

The dissolution amounts of various cation concentrations (Equation 2) were found to be in the following descending order: $Mg^{2+} > Al^{3+} > Fe^{3+} > K^+ > Ca^{2+}$ (Fig. 4 & Table 2). The dissolution amounts of $Al^{3+}$, $Fe^{3+}$ and $Mg^{2+}$ increased with increasing acid concentration. When the oxalic acid concentration was 0.05 M, the dissolution amounts of $Al^{3+}$, $Fe^{3+}$ and $Mg^{2+}$ were 0.77%, 0.56% and 0.91%, respectively. When the oxalic acid concentration was 0.25 M, the dissolution amounts of $Al^{3+}$, $Fe^{3+}$ and $Mg^{2+}$ were 1.49%, 1.06% and 2.56%, respectively. $Mg^{2+}$ was found to be leached more easily than $Fe^{3+}$ from octahedral sheets. The dissolution amounts of $K^+$ and $Ca^{2+}$ underwent slight changes with increasing oxalate concentration. The $K^+$ content of the interlayer cations of phlogopite was small and was not exchanged, and the dissolution amount was only 0.15–0.28%. Each layer in clay minerals has a stable structure because the sheets are bound to each other with covalent bonds (İşçi, 2017). However, water and interlayer cations are bound to the sheets *via* weak van der Waals bonds (Argüelles *et al.*, 2010). Therefore, the

interlayer cations of vermiculite ($Ca^{2+}$) should be leached more easily. However, the $Ca^{2+}$ content in the solution was found very small (0.08–0.12%). The reaction of dissolved $Ca^{2+}$ with oxalic acid to form calcium oxalate precipitate can explain this low $Ca^{2+}$ content in the solution.

After ICP-AES analysis was carried out for the filtrate of samples at various acid leaching durations, the dissolution amounts of $Al^{3+}$, $Mg^{2+}$ and $Ca^{2+}$ were calculated according to Equation 2 and the average dissolution rate of each duration was calculated as shown in Fig. 5. $Al^{3+}$, $Mg^{2+}$ and $Ca^{2+}$ ions occupy tetrahedral, octahedral and interlayer positions in the vermiculite structure, respectively. The rate of metal cation dissolution of vermiculite should, therefore, be in the following descending order: interlaminar > octahedral > tetrahedral, and the dissolution rate of $Mg^{2+}$ should be greater than that of $Al^{3+}$. The dissolution rate of cations is related to the strength of chemical bond; the tetrahedral and octahedral layers are connected by covalent bonds, whereas the interlayer cations and water molecules are connected to the sheets by van der Waals forces, which are weaker than covalent bonds, so cation exchange and dissolution are more likely to occur.

The dissolution rate of $Ca^{2+}$ should be greater than that of Mg and $Al^{3+}$. Because dissolved $Ca^{2+}$ ions react with oxalate ions to form a calcium oxalate precipitate, only a small amount of $Ca^{2+}$ ions exists in the solution. There was essentially no $Ca^{2+}$ in the solution after 6 h, indicating that $Ca^{2+}$ in the solution did not completely form calcium oxalate in the first 6 h and the $Ca^{2+}$ existed in the form of calcium oxalate after 6 h. The characteristic reflections of calcium oxalate were not observed on the XRD traces, but the SEM images showed calcium oxalate crystals attached to the vermiculite surface.

### Cation-exchange capacity

CEC was determined using the ammonium chloride–ethanol exchange method before and after the reaction of the vermiculite sample with the oxalic acid solution (Fig. 6). The measured CEC of vermiculite (130–210 meq 100 g$^{-1}$) was found to be lower than the reported values in the literature, probably due to the presence of interstratified phl-ver. $K^+$ can fit into the ditrigonal cavity of the silicate layer and become more non-exchangeable (Bergaya *et al.*, 2006).
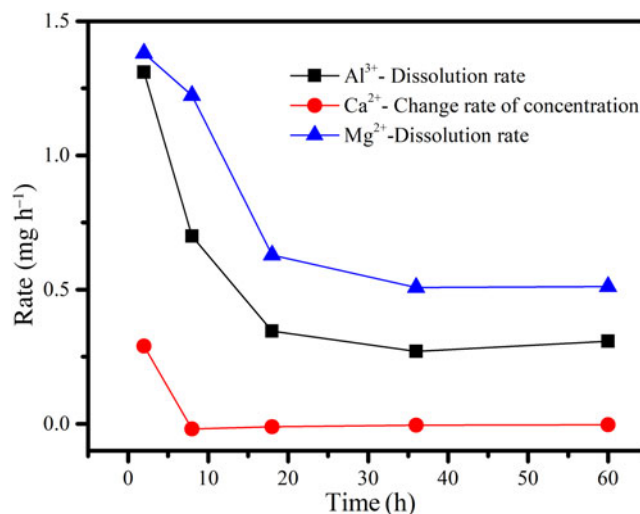
**Table 2.** The dissolution amounts and the dissolution percentages of each cation of Ver-24h-On.

| Oxalate | Al | | Fe | | Mg | | K | | Ca | |
|---|---|---|---|---|---|---|---|---|---|---|
| | $w$ (%) | $w_{Al}$ (%) | $w$ (%) | $w_{Fe}$ (%) | $w$ (%) | $w_{Mg}$ (%) | $w$ (%) | $w_K$ (%) | $w$ (%) | $w_{Ca}$ (%) |
| 0.05 M | 0.77 | 10.88 | 0.56 | 9.43 | 0.90 | 6.78 | 0.15 | 3.70 | 0.08 | 3.58 |
| 0.10 M | 1.13 | 15.97 | 0.80 | 13.43 | 1.77 | 13.32 | 0.21 | 5.08 | 0.10 | 4.40 |
| 0.15 M | 1.29 | 18.32 | 0.92 | 15.52 | 2.14 | 16.06 | 0.23 | 5.60 | 0.10 | 4.39 |
| 0.20 M | 1.43 | 20.26 | 1.02 | 17.17 | 2.43 | 18.24 | 0.26 | 6.27 | 0.09 | 4.06 |
| 0.25 M | 1.49 | 21.07 | 1.06 | 17.84 | 2.55 | 19.13 | 0.28 | 6.93 | 0.12 | 5.44 |



**Figure 5.** Dissolution rates of $Al^{3+}$ and $Mg^{2+}$ and change rate of the $Ca^{2+}$ concentration in the solution.

**Figure 6.** CEC of the vermiculite and products treated with oxalic acid.



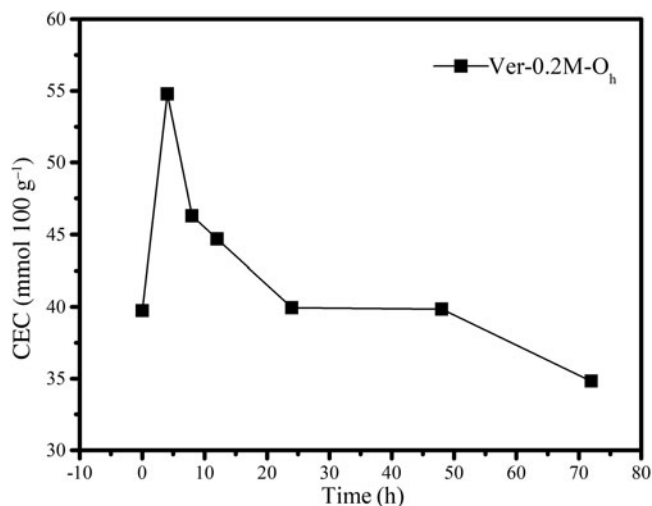**Figure 8.** FTIR spectra of vermiculite and products treated with oxalic acid.

By contrast to the direct decrease of CEC after acid leaching reported by Węgrzyn *et al.* (2018), the CEC of our samples first increased and then decreased with increasing acid treatment duration. This may be due to the high concentration and various types of acids used in the Węgrzyn *et al.* (2018) study. After treatment with 0.2 M oxalate acid for 4, 8 and 12 h, the CEC of the samples increased by 15.0, 6.5 and 4.9 meq 100 $g^{-1}$, respectively. At short reaction durations, $H^+$ interacted with $OH^-$ at the edge or defect positions, causing the octahedron cations to be exposed, which made the internal non-exchangeable cations become exchangeable cations. At longer reaction durations, both exchangeable and non-exchangeable cations were dissolved, causing the CEC to decrease. Therefore, the CEC of vermiculite can be increased by controlling the acid concentration and acid treatment duration.

### Thermal properties

The thermal effects of the original vermiculite on the DSC curves occur primarily in three temperature ranges: 30–200°C, 800–1000°C and 1100–1200°C (Fig. 7a). The endothermic peaks at
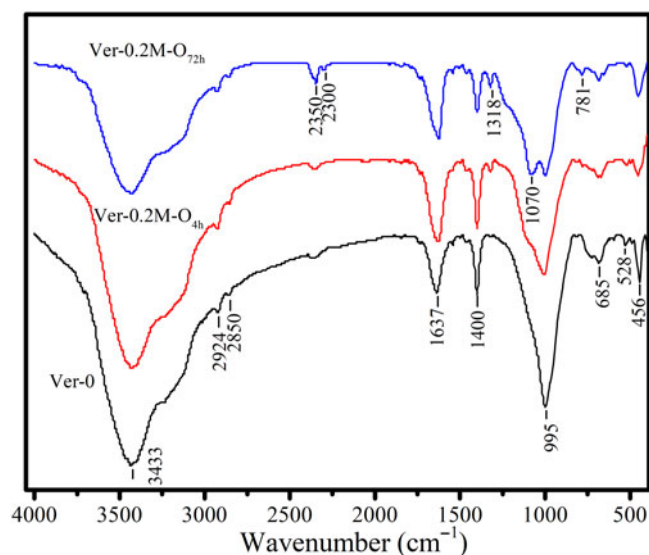
75°C, 103°C and 170°C correspond to the removal of the physically adsorbed and interlayer water molecules (Mouzdahir *et al.*, 2009; Niu *et al.*, 2020). Because the interlayer water of vermiculite was bound with different cations, the stability varied and there were at least three cations between the vermiculite layers. The corresponding weight loss on the TG curve was 6.14%. The endothermic peak at ~828°C could be attributed to the structural water loss and destruction of the structural layer (Silva *et al.*, 2015). The exothermic valley at ~978°C was caused by the crystallization of enstatite from the decomposition products of the vermiculite. The two endothermic peaks and exothermic valleys in the range of ~800–1000°C were not recognized, probably because the original vermiculite sample contains interstratified phl-ver and the absorption/exothermic effects of the two do not overlap. The thermal effect in the range of 1100–1200°C corresponds to the removal of the structural water of phlogopite.

The two endothermic peaks at 101°C and 151°C in the TG-DSC curves of vermiculite correspond to the removal of water molecules bound with various interlayer cations (Fig. 7a). Compared to the original vermiculite, the disappearance of the
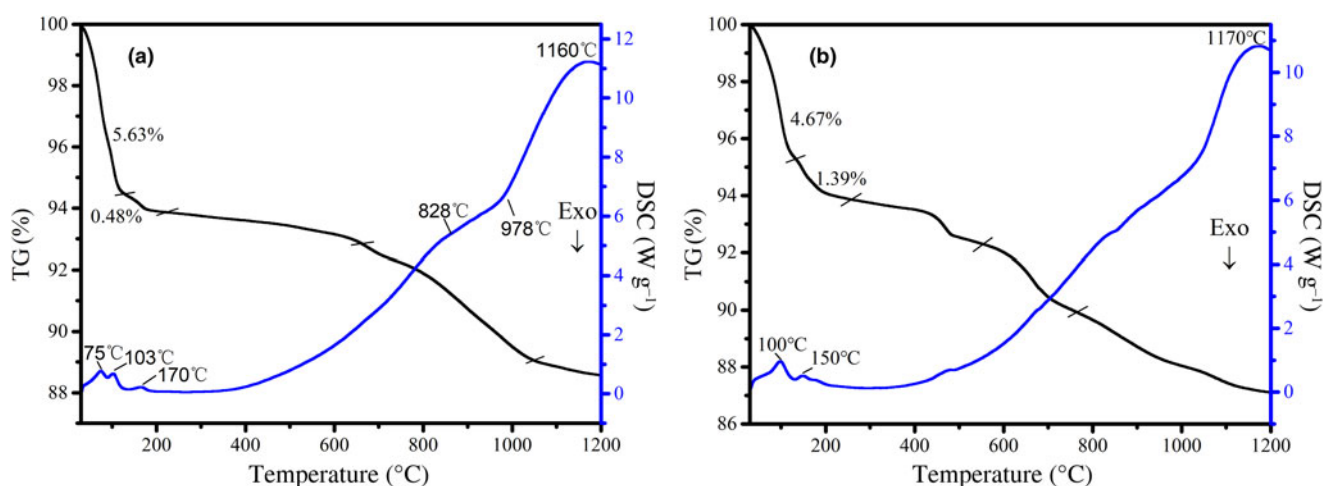


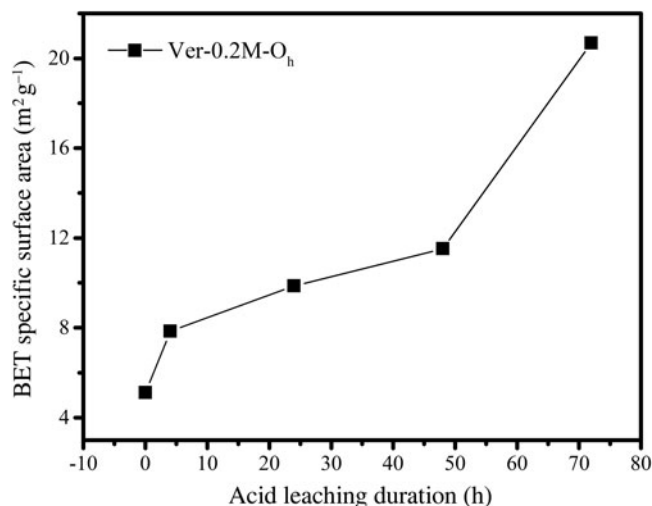**Figure 7.** TG-DSC curves of raw vermiculite and sample Ver-0.2M-O$_{72h}$.

**Figure 9.** Specific surface area of samples leached with 0.2 M $H_2C_2O_4$ solutions.

endothermic peak in leached samples at ~75°C may be attributed to the dissolution of $Ca^{2+}$ (Fig. 7b). The TG curve presented four major weight-loss stages: (1) from 30°C to 200°C, the physical adsorption water and crystal water are removed; (2) from 400°C to 500°C, this stage is due to the decomposition of calcium oxalate into calcium carbonate and carbon monoxide; (3) from 500°C to 700°C, this stage is attributed to the decomposition of calcium carbonate into calcium oxide and carbon dioxide; and (4) from 700°C to 1200°C, this stage is due to the dehydroxylation of vermiculite and phlogopite.

### Infrared characteristics

The FTIR spectra of the original vermiculite sample and the product of the 0.2 M oxalate–vermiculite interfacial reaction are shown in Fig. 8. As the Si–O bond is the strongest bond in the layered silicate mineral structure (Stubican & Roy, 1961), the low-frequency region of 900–1100 $cm^{-1}$ is the characteristic band of layered silicate. The absorption bands in the range of 3750–3200 $cm^{-1}$ are due to the stretching vibration of the H–O–H bonds of water and the structural O–H bonds of vermiculite. Si–O–Si stretching and deformation vibration bands of vermiculite silica tetrahedra appear at 995 and 456 $cm^{-1}$, respectively. While the bands at 725, 685 and 528 $cm^{-1}$ are attributed to the deformation vibration of Al–O–Si bonds of vermiculite (Ritz *et al.*, 2014), the weak band at 3720 $cm^{-1}$ is attributed to O–H stretching vibration bands of vermiculite covered by the O–H stretching vibration band of water at 3433 $cm^{-1}$. After acid
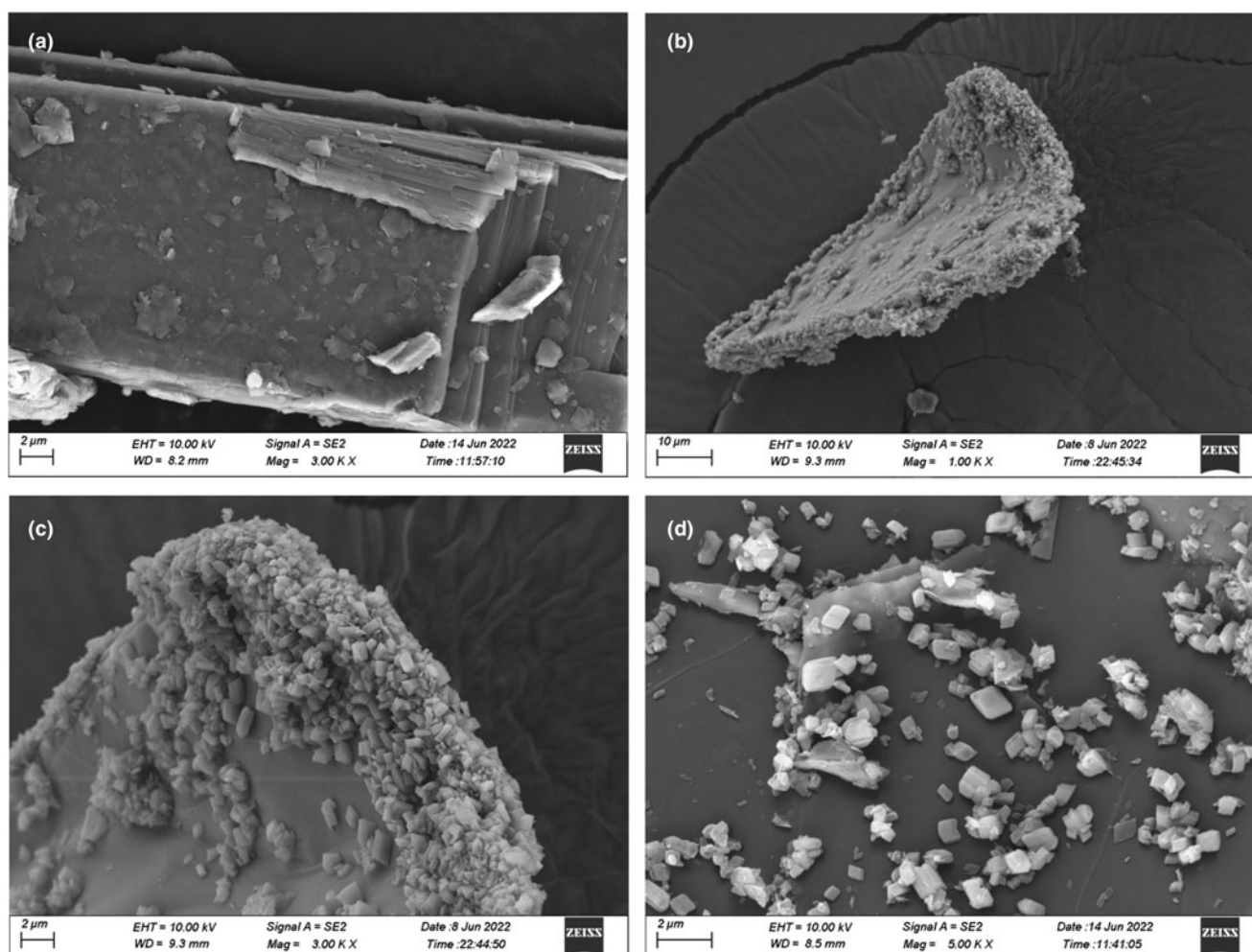


**Figure 10.** SEM images of (a) the original samples and (b–d) after interfacial reaction with 0.2 M oxalate for 72 h.
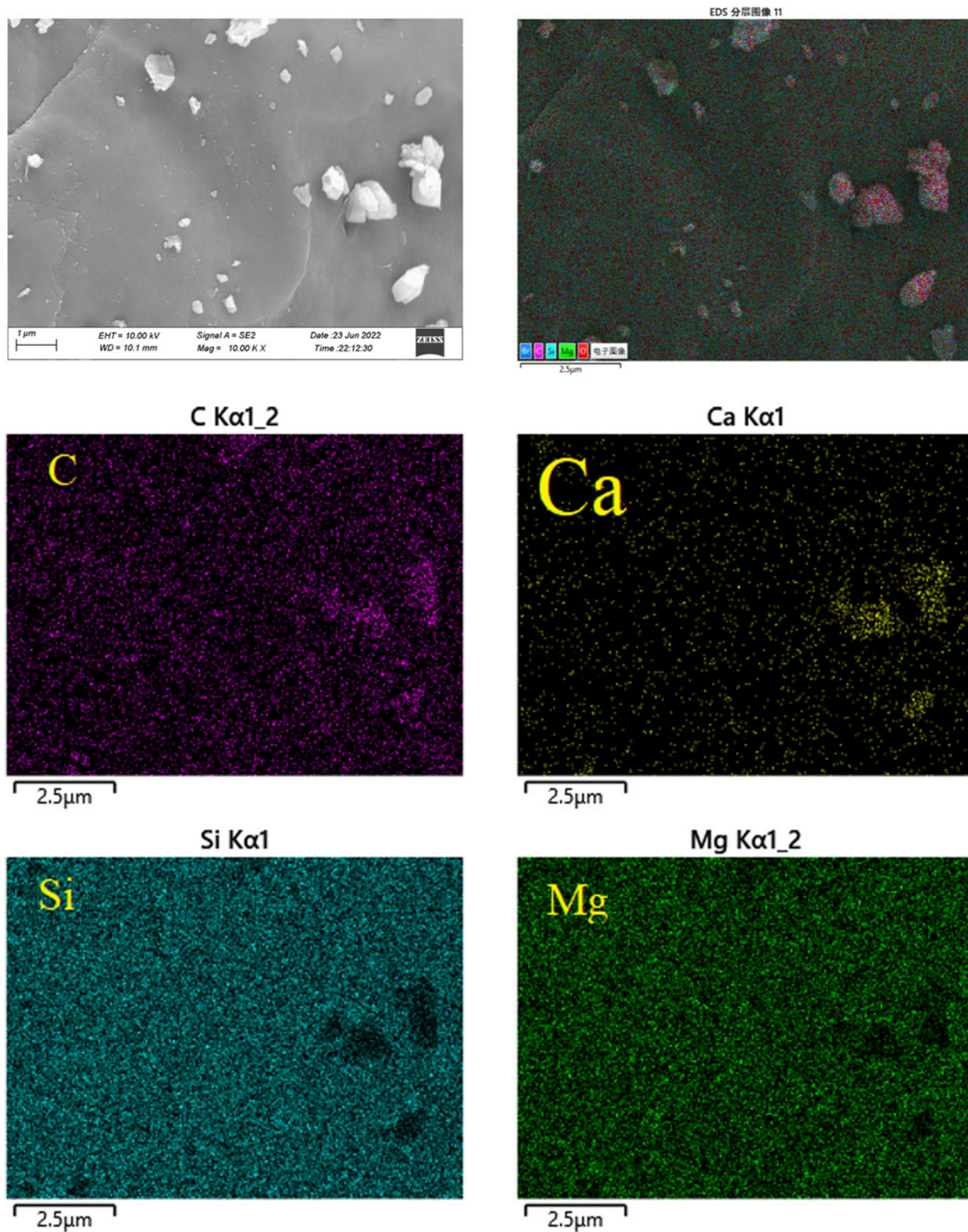
**Figure 11.** EDS images of the original sample and products treated with 0.2 M oxalate.
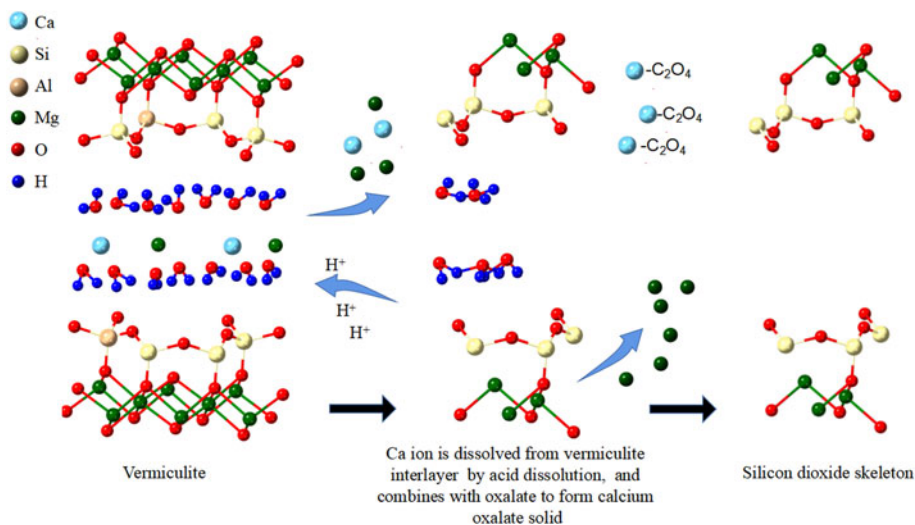
**Figure 12.** Dissolution process of vermiculite in an oxalate environment.

leaching, a 1070 cm$^{-1}$ absorption band was found in the spectra of samples Ver-O$_{72\,h}$. Strong absorption bands at 995 and 456 cm$^{-1}$ of natural vermiculite changed to weaker and wider absorption bands in the spectra of Ver-O$_{72h}$ samples, indicating that the structural order of vermiculite decreased. The band at 1070 cm$^{-1}$ is attribute to stretching vibration of Si–O bonds of amorphous silica, suggesting that the Si–O–Si bonds of the tetrahedra were broken during acid leaching and small amounts of amorphous silica were formed (Komadel *et al.*, 1997). By contrast, Syrmanova *et al.* (2017) reported the formation of substantial amounts of pure silica after reacting vermiculite with 20–25% sulfuric acid solution. The attenuation of absorption bands at 725, 685 and 528 cm$^{-1}$ in the spectra of Ver-O$_{72h}$ and Ver-O$_{4h}$ samples is attributed to the dissolution of Al. The stretching bands of metal hydroxide groups appeared at 1316 and 781 cm$^{-1}$ in the spectra of Ver-O$_{4h}$ samples, indicating the existence of calcium oxalate.

### Specific surface area

Extending the interfacial reaction duration increased the specific surface area of vermiculite gradually (Fig. 9). After acid leaching for 4, 24, 48 and 72 h, the specific surface area of the original vermiculite sample increased from 5.11 m$^2$/g to 7.85, 9.86, 11.51 and 20.07 m$^2$ g$^{-1}$, respectively. Acid leaching caused ions to dissolve and then pores, amorphous silica and calcium oxalate to form, resulting in greater specific surface area.

### Morphological changes and dissolution process

The original vermiculite displayed a clear layered structure with smooth surfaces (Fig. 10a). Many white rhomboid particles were attached to the edges and surfaces of vermiculite after the interfacial reaction (Fig. 10b–d). The SEM-EDS element distribution diagram of the vermiculite surface indicates that the white particles are mainly C and Ca, and there were almost no Si and Mg elements (Fig. 11). The distribution of the particles was greater along the edges and lesser on the surfaces, indicating that the etching process is prone to start from edges and other defect regions.

The dissolution process of vermiculite in an oxalate environment is shown in Fig. 12. The raw vermiculite has a TOT structure, with Ca, Mg and water molecules occupying the interlayer spacing. The basal spacing of vermiculite increases when it adsorbs more water molecules (Zhu *et al.*, 2008). When the interlayer cations of vermiculite dissolved, the interlayer spacing decreased. First, calcium oxalate precipitated on the surface of vermiculite because the dissolved interlayer Ca reacted with the oxalate. Then, Mg ions in the octahedral sheets dissolved, causing the octahedral sheet to be destroyed. Finally, the Si–O–Si bonds in the Si–O tetrahedra were broken, leading to the formation of amorphous silica.

### Conclusion

The dissolution amounts of cations at the oxalic acid interface of vermiculite follow the order: Mg$^{2+}$ > Al$^{3+}$ > Fe$^{2+}$ > K$^+$ > Ca$^{2+}$, indicating that the dissolution difficulty of cations at different structural positions follows the order: interlayer cations > octahedral cations > tetrahedral cations. In addition, Mg$^{2+}$ is more soluble than Fe$^{3+}$ in octahedral sheets. The coupling effect of oxalate causes Ca$^{2+}$ to form a calcium oxalate precipitate, which becomes attached to the edges and surfaces of vermiculite. Furthermore, the distribution of the precipitate was denser along the edges and less dense on the surfaces of vermiculite, indicating that the acid etching process started from the edges and other regions containing structural defects. Due to the formation of amorphous silica and calcium oxalate, the specific surface area of vermiculite increases after interfacial reactions. Increasing the acid leaching duration caused the CEC of the samples first to increase and then to decrease.

**Conflicts of interest.** The authors declare none.

**Consent for publication.** The authors declare their consent for publication.

### References

Argüelles A., Leoni M., Blanco J.A. & Pascual C.M. (2010) Semi-ordered crystalline structure of the Santa Olalla vermiculite inferred from X-ray powder diffraction. *American Mineralogist*, **95**, 126–134.

Bailey S.W. (1980) Summary of recommendations of AIPEA nomenclature committee on clay minerals. *Clay Minerals*, **15**, 85–93.

Bergaya F., Lagaly G. & Vayer M. (2006) Cation and anion exchange. Pp. 979–1001 in: *Developments in Clay Science*, vol. 1 (F. Bergaya, B.K.G. Theng & G. Legaly, editors). Elsevier, Amsterdam, The Netherlands.

Chambi-Peralta M.M., Coelho A.C.V., Carvalho F.M.d.S. & Toffoli S.M. (2018) Effects of exchanged cation, acid treatment and high shear mechanical treatment on the swelling and the particle size distribution of vermiculite. *Applied Clay Science*, **155**, 1–7.

Christidis G E. (2008) Validity of the structural formula method for layer charge determination of smectites: a re-evaluation of published data. *Applied Clay Science*, **42**, 1–7.

del Rey-Perez-Caballero F.J. & Poncelet G. (2000) Microporous 18 Å Al-pillared vermiculites: preparation and characterization. *Microporous and Mesoporous Materials*, **37**, 313–327.

Frini-Srasra N. & Srasra E. (2010) Acid treatment of south Tunisian palygorskite: removal of Cd(II) from aqueous and phosphoric acid solutions. *Desalination*, **250**, 26–34.

Guggenheim S., Adams J.M., Bain D.C., Bergaya F., Brigatti M.F., Drits V.A. *et al.* (2006) Summary of recommendations of nomenclature committees relevant to clay mineralogy: report of the Association Internationale pour l'Etude des Argiles (AIPEA) Nomenclature Committee for 2006. *Clay Minerals*, **41**, 863–877.

He H.P., Cao J.L. & Duan N. (2019) Defects and their behaviors in mineral dissolution under water environment: a review. *Science of the Total Environment*, **651**, 2208–2217.

İşçi S. (2017) Intercalation of vermiculite in presence of surfactants. *Applied Clay Science*, **146**, 7–13.

Komadel P., Janek M., Madejova J., Weekesb A. & Breen C. (1997) Acidity and catalytic activity of mildly acid-treated Mg-rich montmorillonite and hectorite. *Physical Chemistry Chemical Physics*, **93**, 4207–54242.

Ma L., Su X., Xi Y., Wei J., Liang X., Zhu J. & He H. (2019) The structural change of vermiculite during dehydration processes: a real-time *in-situ* XRD method. *Applied Clay Science*, **183**, 105332.

Maqueda C., Romeroa A.S., Morilloa E. & Pérez-Rodrєguez J.L. (2007) Effect of grinding on the preparation of porous materials by acid-leached vermiculite. *Journal of Physics and Chemistry of Solids*, **68**, 1220–1224.

Maqueda C., Perez-Rodriguez J.L., Šubrt J. & Murafa N. (2009) Study of ground and unground leached vermiculite. *Applied Clay Science*, **44**, 178–184.

Mittal V. (2013) High CEC generation and surface modification in mica and vermiculite minerals. *Philosophical Magazine*, **93**, 777–793.

Mouzdahir Y.E., Elmchaouri A., Mahboub R., Gil A. & Korili S.A. (2009) Synthesis of nano-layered vermiculite of low density by thermal treatment. *Powder Technology*, **189**, 2–5.

Niu H., Kinnunen P., Sreenivasan H., Adesanya E. & Illikainen M. (2020) Structural collapse in phlogopite mica-rich mine tailings induced by mechanochemical treatment and implications to alkali activation potential. *Minerals Engineering*, **151**, 106331.

Putnis C.V. & Ruiz-Agudo E. (2013) The mineral–water interface: where minerals react with the environment. *Elements*, **9**, 177–182.

Ritz M., Zdrálková J. & Valášková M. (2014) Vibrational spectroscopy of acid treated vermiculites. *Vibrational Spectroscopy*, **70**, 63–69.

Silva F.M.N., Silva E.L., Anjos I.F., Fontgalland G. & Rodrigues M.G.F. (2015) Characterization of natural clay vermiculite, expanded by indirect method for energy and microwave. *Materials Science Forum*, **820**, 36–39.

Steudel A., Batenburg L.F., Fischer H.R., Weidler P.G. & Emmerich K. (2009) Alteration of swelling clay minerals by acid activation. *Applied Clay Science*, **44**, 105–115.

Stubican V. & Roy R. (1961) Infrared spectra of layer-structure silicates. *Journal of the American Ceramic Society*, **44**, 625–627.

Su H. & Zhou W. (2020) Mechanism of accelerated dissolution of mineral crystals by cavitation erosion. *Acta Geochimica*, **39**, 11–42.

Suquet H., Chevalir S., Marcily C. & Barthomeuf D. (1991) Preparayion porous materials by chemical activation of the LLANO vermiculite. *Clay Minerals*, **26**, 49–60.

Syrmanova K., Suleimenova M.T., Kovala A., Botabayev Y. & Kaldybekova Z.B. (2017) Vermiculite absorption capacity increasing by acid activation. *Oriental Journal of Chemistry*, **33**, 509–513.

Temuujin J., Okada K., Kenneth J.D. & MacKenzie K.J.D. (2003) Preparation of porous silica from vermiculite by selective leaching. *Applied Clay Science*, **22**, 187–195.

Victoria K., Sergey Z., Ekaterina T., Olga D., Anatoliy Z., Petr B. & Maria T. (2017) Experimental study of montmorillonite structure and transformation of its properties under treatment with inorganic acid solutions. *Minerals*, **7**, 49.

Warren C.J., Dudas M.J. & Abboud S.A. (1992) Effects of acidification on the chemical composition and layer charge of smectite from calcareous till. *GeoScienceWorld*, **40**, 731–739.

Węgrzyn A., Stawiński W., Freitas O., Komędera K., Błachowski A., Jęczmionek Ł. *et al.* (2018) Study of adsorptive materials obtained by wet fine milling and acid activation of vermiculite. *Applied Clay Science*, **155**, 37–49.

White A.F. & Brantley S.L. (2003) The effect of time on the weathering of silicate minerals: why do weathering rates differ in the laboratory and field? *Chemical Geology*, **202**, 479–506.

Zhu R., Zhu L., Zhu J. & Xu L. (2008) Structure of cetyltrimethylammonium intercalated hydrobiotite. *Applied Clay Science*, **42**, 224–231.